Sea level change from BeiDou Navigation Satellite System-Reflectometry (BDS-R): First results and evaluation

CrossMark

Shuanggen Jin [a,*], Xiaodong Qian [a,b], X. Wu [a]

[a] Shanghai Astronomical Observatory, Chinese Academy of Sciences, Shanghai 200030, China
[b] University of Chinese Academy of Sciences, Beijing 100047, China

ARTICLE INFO

ABSTRACT

Sea level changes affect human living environments, particularly ocean coasts. The tide gauges (TG) can measure sea level change, while it is the relative variations with respect to the land. Recently, GPS-Reflectometry (GPS-R) has been demonstrated to measure sea level change as an altimetry. With the rapid development of China's BeiDou Navigation Satellite System (BDS), it may provide a new possible opportunity to monitor sea level changes with three frequencies (L2, L6 and L7). In this paper, BDS-Reflectometry (BDS-R) is the first time used to estimate the sea level changes based on Signal-to-Noise Ratio (SNR) data and triple-frequency phase and code combinations, which are compared to tide gauge observations. Results show that sea level changes from BDS SNR and phase combination have a good agreement with correlation coefficients of 0.83–0.91 and RMSEs of less than 0.6 m, while BDS code combination is not as good as others. Furthermore, a new negative linear model between phase and code peak frequencies and tide gauge observations is further obtained and analyzed, which improves the results from three-frequency phase and code combinations with the RMSE of about 10 cm and 18 cm.

© 2016 Elsevier B.V. All rights reserved.

1. Introduction

Recent global climate change is resulting in sea level variations due to glacier melting and thermal expansion (Douglas et al., 2001; Jin et al., 2013), which affect human living environments, especially ocean coasts. Traditionally, sea level changes are measured by the tide gauge (TG), whereas TG provides the relative sea level variations with respect to the TG land (Feng et al., 2013). Recently, GPS-Reflectometry (GPS-R) has been demonstrated to measure sea level change, soil moisture, and snow depth (Jin et al., 2011; Löfgren et al., 2011; Najibi and Jin, 2013). Compared to the typical tide gauge, GPS can determine absolute sea level change since GPS can measure the land motion. Based on the multipath reflectometry theory, sea level changes can be measured by geodetic GNSS receivers, but most used the GPS or GLONASS L1 and L2 SNR data (Larson et al., 2012; Lofgren et al., 2014). In addition, GNSS multipaths extracted by the L4 linear combination can also estimate snow depth (Jin et al., 2014). Therefore, three-frequency phase combination and L4 linear combination of GPS measurements are possibly used to estimate sea level changes.

With the rapid development of China's BeiDou Navigation Satellite System (BDS), it may provide a new possible opportunity to monitor sea level changes with three frequencies (L2, L6 and L7). In this paper,

BDS L2, L6 and L7 SNR data and three-frequency phase and code combinations are the first time used to estimate sea level changes. The BDS results are further evaluated by comparing with tide gauge observations. Some effects are also discussed. Finally, conclusions are given.

2. Observations and methods

2.1. BDS and TG observations

The BeiDou Navigation Satellite System (BDS) has been developed since early 1990s. Currently more than 19 BDS satellites are operating, including Geostationary Earth Orbit (GEO) satellites, Inclined Geosynchronous Orbit (IGSO) satellite and Medium Earth Orbit (MEO) satellites. The BDS provides global and regional positioning, navigation and timing (PNT). Here one IGS Multi-GNSS station MAYG with co-located tide gauge measurements is used to estimate sea level changes, which is located in Mayotte near the Indian Ocean. The MAYG station has installed TRIMBLE NETR9 receiver and TRM59800.00 antenna (latitude: −12.78°, longitude: 45.26° and height: −16.35 m). Because MAYG is one of the Multi-GNSS Experiment (MGEX) stations, it receives not only the GPS and GLONASS signals but also BDS signal with three frequencies (L2, L6 and L7). The five available BDS satellites (PRN (Pseudo Random Noise) 6, 7, 8, 9, and 10) are used estimate sea level change from January 2015 to June 2015. The co-located tide gauge station is Dzaoudzi with about several meters far from the MAYG station. The

* Corresponding author.
E-mail addresses: sgjin@shao.ac.cn, sg.jin@yahoo.com (S. Jin).
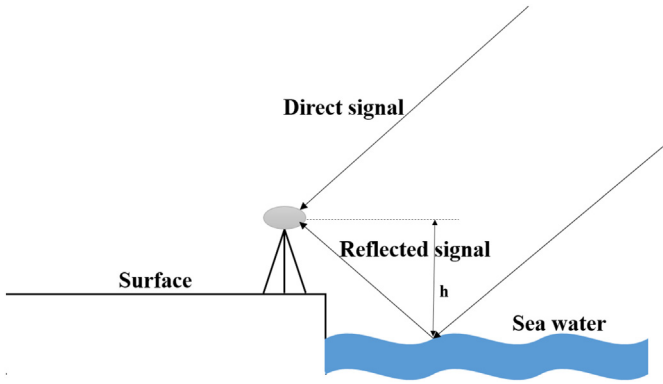
Fig. 1. Geometry of BDS-Reflectometry (BDS-R). The h is the antenna height from reflected surface.

sea level data collected by the radar sensor with sampling rate of 1 min are provided by the Intergovernmental Oceanographic Commission (IOC).

2.2. Signal-Noise to Ratio (SNR) method

The reflected signal has one excess phase delay when compared to the direct signal, also called GNSS multipath, which is related to the antenna height h in Fig. 1. The interference between the direct and reflected signals will affect GNSS observations and cause oscillations in observations. The GNSS oscillations (multipath) in observables can reflect the sea level change.
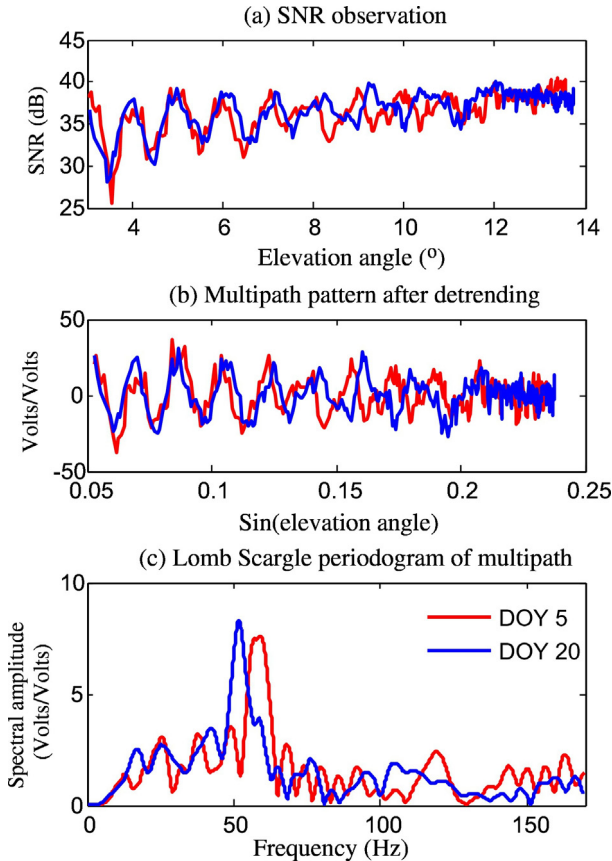
Fig. 2. BDS L7 SNR observation, multipath pattern and Lomb Scargle periodogram for PRN7 satellite.
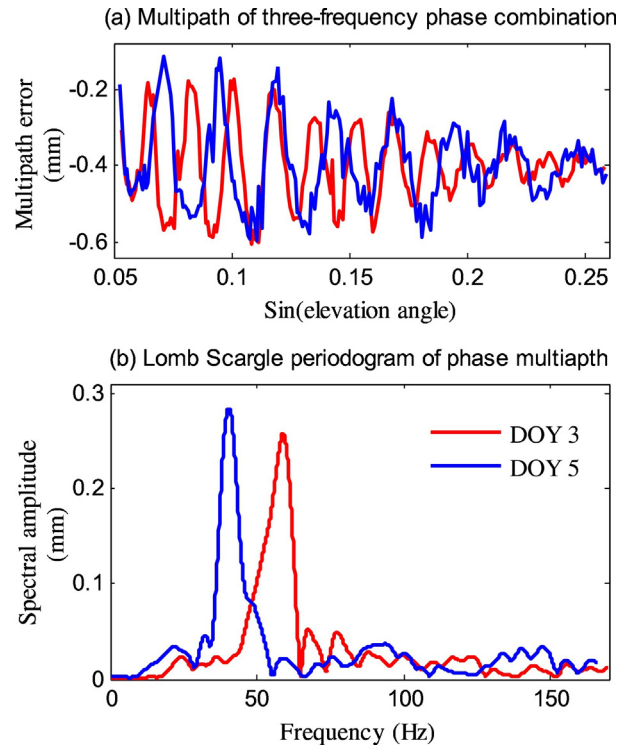
Fig. 3. Multipath error of three-frequency phase combination and Lomb Scargle periodogram for BDS PRN9 satellite.

Signal-Noise to Ratio (SNR) is one of main GNSS observables, which is usually used to assess the signal quality and the noise characteristics of typical GNSS observations. Compared to phase and code observations (Najibi et al., 2015), it is easier to extract multipath from SNR data. The multipath will cause oscillations in SNR observations, see in Fig. 2a. If there is no multipath effect, the SNR observation will rise smoothly with the increasing of elevation angle. In order to extract the multipath, low-order polynomial is used to obtain SNR detrended time series. After removing the SNR trend, the multipath pattern can be obtained and modeled as following (Jin et al., 2016; Qian and Jin, 2016):

$$dSNR = A\cos\left(4\pi h\lambda^{-1}\sin e + \phi\right) \qquad (1)$$

where A is the amplitude, h is the antenna height from the reflected surface in Fig. 1, λ is the carrier wavelength, e is the elevation angle and ϕ is the phase. Supposed that the reflector height h in Fig. 1 does not change during the period of satellite arc and the reflected surface is horizontal, the frequency of multipath
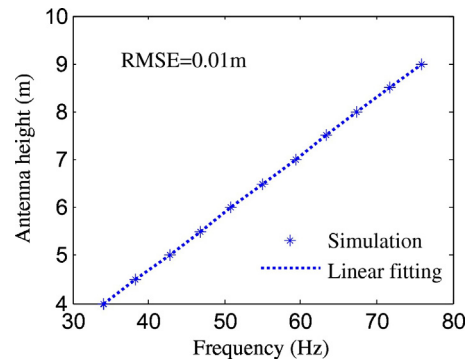
Fig. 4. Linear relationship between peak frequencies and antenna heights.
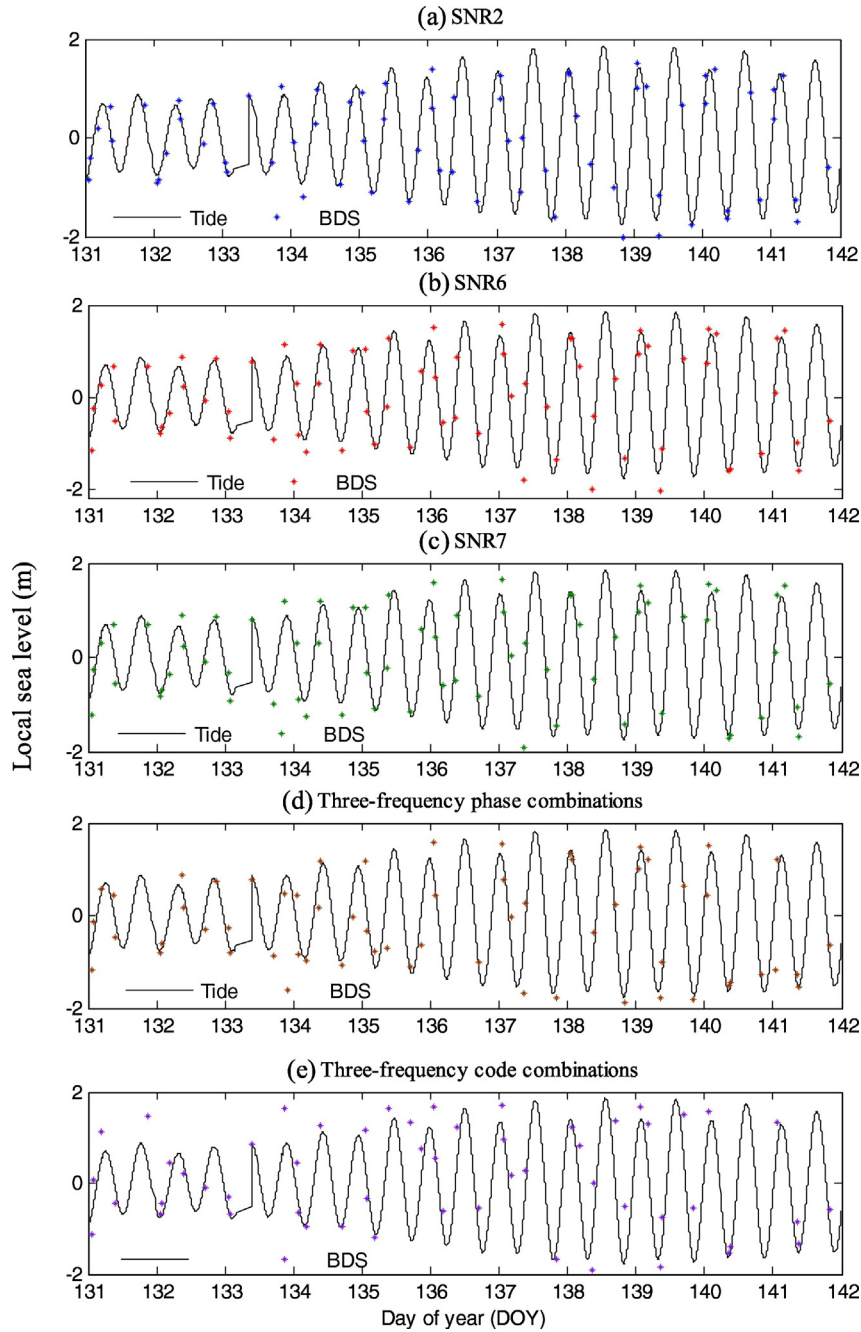
Fig. 5. Sea level changes from BDS L2, L6 and L7 SNR, three-frequency combinations and tide gauge observations for 10 days.

pattern is a constant with respect to the Sine of satellite elevation angle. Though the sea level changes with the time, this constant frequency model is sufficient for this station whose maximum tide range is 4 m, which is less than the tide range 7 m that should consider the varying reflector height (Larson et al., 2013). Through Eq. (1), the frequency of multipath pattern can be obtained as following

$$h = \frac{1}{2}\lambda f \qquad (2)$$

where f is the frequency of multipath pattern, λ is carrier wavelength and h is the antenna height. From Eq. (2), it is clear to see that the high multipath frequency corresponds to one large reflector height in Fig. 1, meaning a low sea level. In contrast, a high sea level corresponds to a low multipath frequency. The dominant frequency of multipath can be derived from the dSNR data by a spectrum analysis. In this paper, we use the Lomb Scargle method to covert the data to frequency domain and obtain the dominant frequency (Qian and Jin, 2016). From Fig. 2b and c, the frequencies of multipath patterns are different, so different peak heights reflect sea level changes.

2.3. Three-frequency combination

For phase and code observables, it is difficult to directly extract multipath from observations. However, the linear combination between observations can extract the multipath, such as phase and code combination, L4 linear combination and three-frequency combination. Compared to double-frequency linear combination,
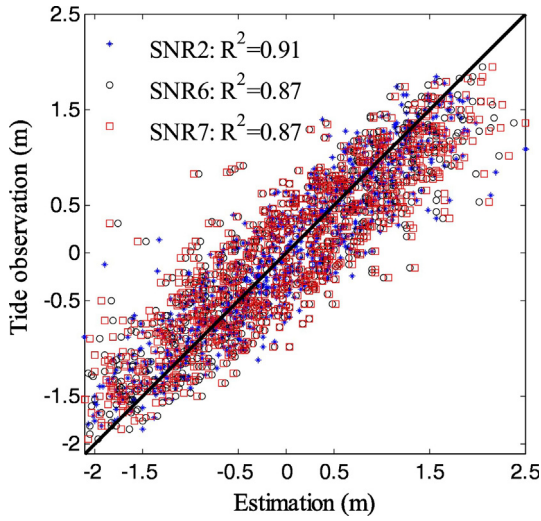
Fig. 6. Correlation of BDS L2, L6 and L7 SNR estimations with tide gauge observations.
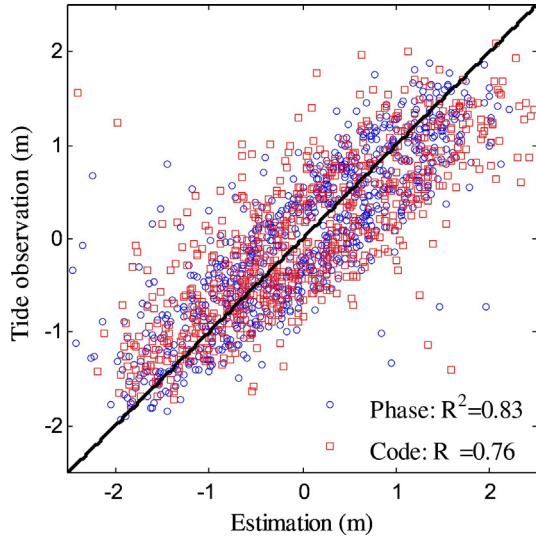
Fig. 7. Correlation of BDS three-frequency phase and code combinations' estimations with tide gauge observations.
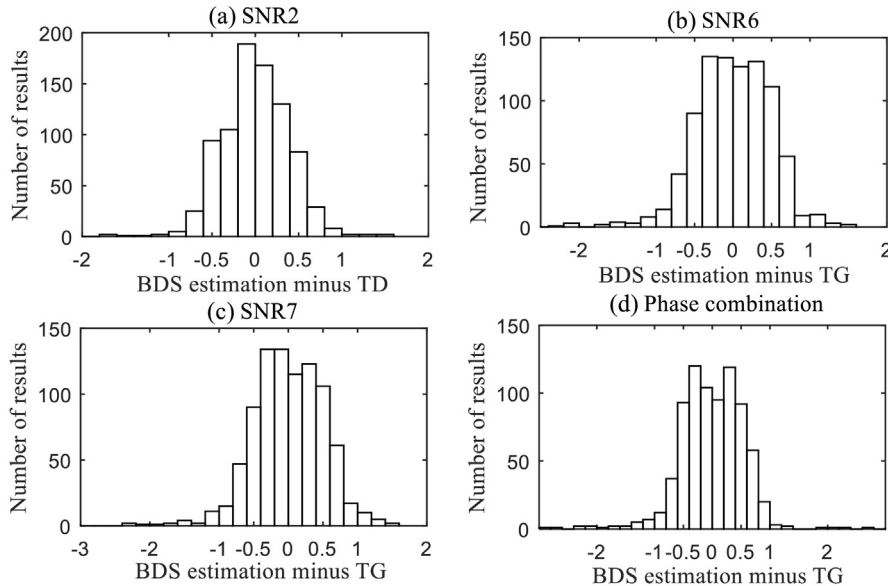
three-frequency linear combination has an advantage to cancel the second-order ionospheric delay error. Phase multipath from three-frequency GNSS observations is given as follow (Simsky, 2006):

$$MP_\varphi = \lambda_3^2(\varphi_1\text{-}\varphi_2) + \lambda_2^2(\varphi_3\text{-}\varphi_1) + \lambda_1^2(\varphi_2\text{-}\varphi_3) \tag{3}$$

where λ_1, λ_2 and λ_3 are the wavelengths of three-frequency carriers and φ_1, φ_2 and φ_3 are the phase observations with length unit. For BDS, the three-frequency carriers are L2, L6 and L7. The structure of pseudorange combination is same with phase term described as following

$$MP_p = \lambda_3^2(P_1\text{-}P_2) + \lambda_2^2(P_3\text{-}P_1) + \lambda_1^2(P_2\text{-}P_3) \tag{4}$$

where P_1, P_2 and P_3 are the pseudorange observations. From Eq. (3) and (4), three-frequency multipath errors are mainly the combination of single phase or range errors. For phase multipath, a phase shift related to the total received signals (i.e., reflected plus direct ones) can be modeled as following (Jin and Najibi, 2014)

$$\delta\phi = \tan^{-1}\left(\frac{\alpha \sin\left(4\pi h\lambda^{-1}\sin e\right)}{1 + \alpha \cos\left(4\pi h\lambda^{-1}\sin e\right)}\right) \tag{5}$$

where α is the reflection coefficient depending on the reflectivity of the reflected surface and the antenna gain pattern, h is the antenna height, λ is the wavelength and e is the elevation angle. From Eq. (5), the phase multipath is quasi-periodical and its frequency is also related to the antenna height. Because three-frequency multipath errors are the combination of single phase or range errors, the combination error should be also quasi-periodical including three different frequencies for different carrier phases. However, when the combined multipath error is converted into the frequency domain, there is only one peak height (Fig. 3b). This is probably because BDS L6 and L7 wavelengths are so similar that the scaling factor for the L2 term is much smaller than those for the L6 and L7 terms. In Fig. 3, three-frequency phase multipath errors from different days have different frequencies, which is the same as SNR results.

After obtaining the frequency of multipath, another important step is to convert the frequency to the reflector height. We use the simulator presented by Nievinski and Larson (2014) to model the combined phase

Fig. 8. Residual between BDS SNR and three-frequency phase estimations with tide gauge observations.

and code errors and then fit the relationship between the frequencies and supposed reflector heights. The reflector heights are about between 4 m and 9 m at MAYG station, so we supposed a series of antenna heights between 4 m and 9 m during the simulation. Fig. 4 shows the relationship between antenna heights and peak frequencies during the specific elevation range (5°–18°). It can be seen a linear relationship as

$$h = 0.1202 \times f - 0.1154 \qquad (6)$$

where h is the antenna height and f is the peak frequency of combined multipath errors. If using the BDS L6 (0.2363 m) or L7 (0.2483) wavelength as the parameter in Eq. (2), the relationship is close to Eq. (6). Following the same procedure, the relationship for code combination can also be obtained as

$$h = 0.1204 \times f - 0.1286 \qquad (7)$$

After obtaining the peak frequency of combined phase or code multipath, the antenna height or sea level change can be calculated using Eq. (6) and Eq. (7).

3. Results and analysis

Before obtaining the peak frequency, the BDS SNR, phase and code observations are clustered into ascending or descending sections according to the satellite track and azimuth. In this paper, observations are used only below 18° elevation angle because they are easily affected by the multipath at this station. Furthermore, since the sea level change is focused in this paper, the signals reflected from the sea surface are used. Through evaluating the map around the station and the reliability of the observations, tracks just between the azimuths of 20° to 80° and 110° to 170° are used to perform the spectral analysis. Since co-located tide gauge observations are not measured by every second, the interpolation is used to get the observation at one time corresponding to the antenna height, which is derived from the given track.

When comparing the BDS-derived sea level results with in-situ observations from tide gauge, the different references for sea level series should be considered. The BDS-derived sea level changes are relative to the BDS station, while the tide gauge sea level observations are relative to the tide gauge benchmark. Therefore, a mean sea level will be obtained by comparing the difference between BDS-derived results and tide gauge observations. Fig. 5 shows 10-day sea level change time series. It can be seen that the BDS-derived results have a good agreement with tide gauge observations, although results from three-frequency code combination are not as good as others. Because of limited BDS satellites, the number of estimations is not as much as that from GPS (Lofgren et al., 2014). In addition, BDS-derived sea level series also show semi-diurnal variations at Dzaoudzi tide station. Figs. 6 and 7 show the correlations of BDS results with tide gauge observations with a good correlation. Fig. 8 shows the residuals between BDS SNR and phase estimations with tide gauge observations. It is clear to see that results from SNR2 data with a RMSE of 0.39 m are better than those from the others. Table 1 presents detailed correlation and RMSE values for BDS-derived results.

4. Discussions

4.1. Comparison with GPS results

One new signal, called L5, has also been broadcasted by GPS block IIF satellites since 2010, so GPS with three frequency observations is also used to estimate sea level change. In this paper, GPS-derived results from PRN 1, 3, 6, 9, 24, 25, 27 and 30 satellites are compared to results from BDS (Table 1). Fig. 8 shows the residuals between GPS-

Table 1
The correlation and RMSE for BDS and GPS-derived results with TG.

System	Observation	Correlation	RMSE (m)
BDS	SNR2	0.91	0.39
	SNR6	0.87	0.49
	SNR7	0.87	0.52
	Phase	0.83	0.56
	Code	0.76	0.69
GPS	SNR2	0.82	0.56
	SNR5	0.87	0.43
	Phase	0.87	0.46
	Code	0.84	0.49

derived results with tide gauge observations. The estimations from GPS SNR5 with the correlation of 0.87 and RMSE of 0.43 m are better than the others. Also results from three-frequency GPS phase and code combinations are poorer than that from SNR, which is same as BDS's results. It denotes that the linear model is not precise. In Table 1, there are no results from GPS L1 SNR data because of its poor performance, which may be caused by some other errors at this site. From Table 1, there are some little differences between results from GPS and BDS, which are caused by different reflection areas. Fig. 9 shows multipath reflection points for GPS and BDS on Jan 2, 2015 at MAYG. In this paper, the azimuth of interested areas is used from 20° to 80° and 110° to 170°. Most tracks of BDS are among these areas, while some tracks of GPS are not available. In addition, the areas covered by GPS and BDS are different, which may cause some differences.

4.2. Linear model improvement

From Fig. 8 and Table 1, results from three-frequency phase and code combinations are not as good as that from SNR2 and SNR6. Basically, the carrier phase is the most precise observables in GNSS measurements, so results from three-frequency phase combination should be as good as that from SNR although there are some other errors. In Section 2.3, we know the linear relationship between peak frequency and antenna height is not precise because it is just derived from the simulation results. The simulations cannot represent the real situation for this station although it considers the coherence between the direct and reflected signals, and the combinations of antenna and surface responses. Some other factors like sea water roughness and composition will affect the reflected signals. Therefore, the accurate linear relationship will improve the results from three-frequency combinations. Through simulations, the relationship between peak frequency and antenna height is a linear model, so the relationship between peak frequency and tide gauge observations should be also linear basically. After fitting the

Fig. 9. Multipath reflection points for GPS and BDS on Jan. 2, 2015 at MAYG.

(a) Relationship between phase peak frequency and observation

RMSE=0.45m
y= -0.094x+6.989

(b) Relationship between code peak frequency and observation

RMSE=0.51m
y= -0.078x+6.114
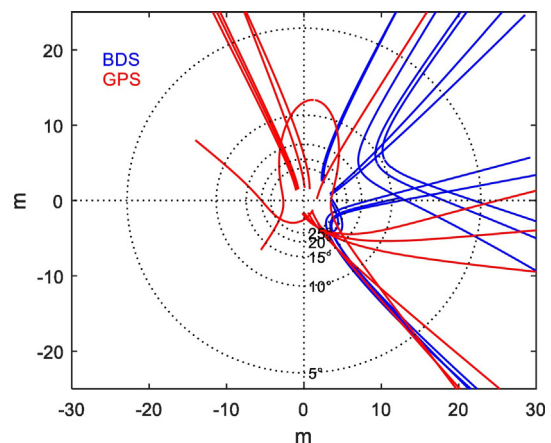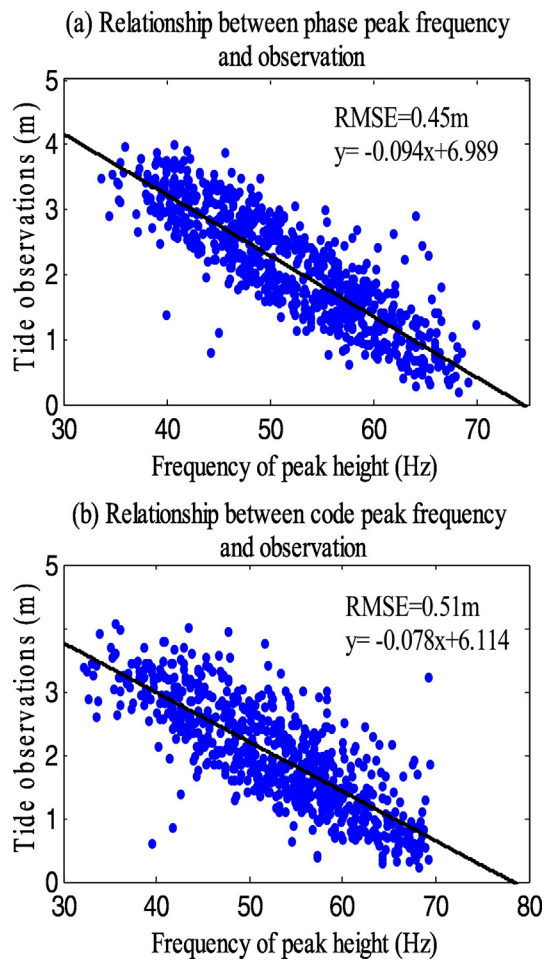
Fig. 10. Relationship between BDS phase-code peak frequencies and tide gauge observations.

code and phase peak frequencies with tide gauge observations, it is clear that there is one negative linear relationship between them (Fig. 10). While using the negative linear model to convert the peak frequencies to sea levels, results are better than that using simulated linear model with the RMSE of 0.45 m for phase and the RMSE of 0.51 m for code.

5. Conclusion

In this paper, BDS SNR data and three-frequency phase and code combinations are the first time used to estimate sea level changes at MAYG station, which shows a good agreement with Tide Gauge observations, while results of BDS code combinations are not as good as others with a low precision. After fitting the code and phase peak frequencies with tide gauge observations, a new negative linear model between phase and code peak frequencies and tide gauge observations is obtained, which greatly improves the results from three-frequency phase and code combinations with RMSE of about 10 cm and 18 cm.

References

Douglas, B.C., Kearney, M.S., Leatherman, S.P., 2001. Sea Level Rise: History and Consequences. Academic, San Diego, CA.
Feng, G.P., Jin, S.G., Zhang, T.Y., 2013. Coastal sea level changes in the Europe from GPS, Tide Gauge, Satellite Altimetry and GRACE, 1993–2011. Adv. Space Res. 51 (6): 1019–1028. http://dx.doi.org/10.1016/j.asr.2012.09.011.
Jin, S.G., Najibi, N., 2014. Sensing snow height and surface temperature variations in Greenland from GPS reflected signals. Adv. Space Res. 53 (11), 1623–1633.
Jin, S.G., Feng, G., Gleason, S., 2011. Remote sensing using GNSS signals: current status and future directions. Adv. Space Res. 47 (10), 1645–1653.
Jin, S.G., van Dam, T., Wdowinski, S., 2013. Observing and understanding the Earth system variations from space geodesy. J. Geodyn. 72:1–10. http://dx.doi.org/10.1016/j.jog.2013.08.001.
Jin, S.G., Cardillach, E., Xie, F., 2014. GNSS Remote Sensing: Theory, Methods and Applications. Springer, p. 276.
Jin, S.G., Qian, X.D., Kutoglu, H., 2016. Snow depth variations estimated from GPS-Reflectometry: a case study in Alaska from L2P SNR data. Remote Sens. 8 (1):63. http://dx.doi.org/10.3390/rs8010063.
Larson, K.M., Lofgren, J.S., Haas, R., 2012. Coastal sea level measurements using a single geodetic GPS receiver. Adv. Space Res. 51 (8), 1301–1310.
Larson, K.M., Ray, R.D., Nievinski, F.G., Freymueller, J.T., 2013. The accidental tide gauge: a GPS reflection case study from Kachemak Bay, Alaska. Geosci. Rem. Sens. Lett. IEEE 10 (5), 1200–1204.
Löfgren, J.S., Haas, R., Johansson, J.M., 2011. Monitoring coastal sea level using reflected GNSS signals. Adv. Space Res. 47 (2), 213–220.
Lofgren, J.S., Haas, R., Scherneck, H.G., 2014. Sea level time series and ocean tide analysis from multipath signals at five GPS sites in different parts of the world. J. Geodyn. 80, 66–80.
Najibi, N., Jin, S.G., 2013. Physical reflectivity and polarization characteristics for snow and ice-covered surfaces interacting with GPS signals. Remote Sens. 5 (8), 4006–4030.
Najibi, N., Jin, S., Wu, X., 2015. Validating the variability of snow accumulation and melting from gps-reflected signals: forward modeling. IEEE Trans. Antennas Propag. 63 (6), 2646–2654.
Nievinski, F.G., Larson, K.M., 2014. An open source GPS multipath simulator in Matlab/Octave. GPS Solutions 18 (3), 473–481.
Qian, X.D., Jin, S.G., 2016. Estimation of snow depth from GLONASS SNR and phase-based multipath reflectometry. IEEE J. Sel. Topics Appl. Earth. Observ. Remote Sens. 9 (10): 4817–4823. http://dx.doi.org/10.1109/JSTARS.2016.2560763.
Simsky, A., 2006. Three's the charm. Triple-frequency combinations in future GNSS. Inside GNSS: GPS, GALILEO, GLONASS, COMPASS. Policies, Programs, Engineering, and Advanced Applications of the Global Navigation Satellite System. 1(5), pp. 38–41.